AD-A064 319 GEORGIA INST OF TECH ATLANTA FRACTURE AND FATIGUE RE--ETC F/G 11/6
FATIGUE CRACK PROPAGATION OF METASTABLE BETA TITANIUM-VANADIUM --ETC(U)
DEC 78 S B CHAKRABORTTY, E A STARKE N00014-75-C-0349

UNCLASSIFIED GIT-TR-78-3 NL

1 OF 1

AD
A064 319

END
DATE
FILMED
4 -79
DDC

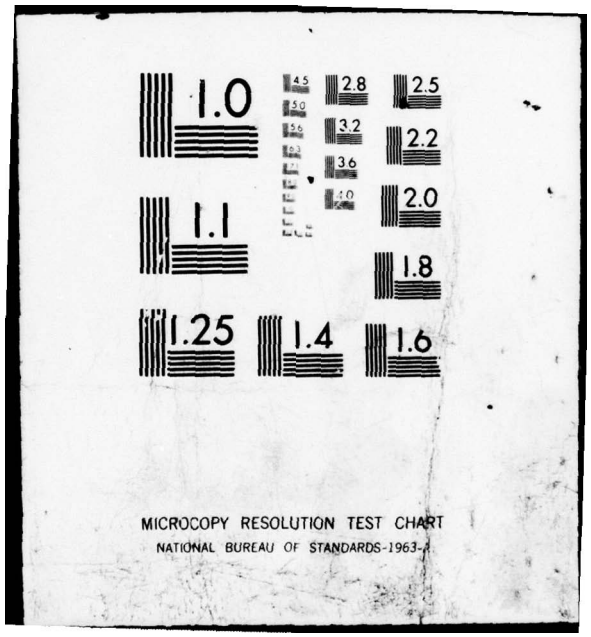
1.0
1.1
1.25
1.4
1.6
1.8
2.0
2.2
2.5
2.8
3.2
3.6
4.0
4.5
5.0
5.6
MICROCOPY RESOLUTION TEST CHART
NATIONAL BUREAU OF STANDARDS-1963-A

LEVEL II

12

B.S.

OFFICE OF NAVAL RESEARCH

Contract N00014-75-C-0349, NR 031-750

TECHNICAL REPORT 78-3

FATIGUE CRACK PROPAGATION OF METASTABLE BETA TITANIUM-VANADIUM ALLOYS

By
Saghana B. Chakrabortty and Edgar A. Starke, Jr.

December 7, 1978

FRACTURE AND FATIGUE RESEARCH LABORATORY
GEORGIA INSTITUTE OF TECHNOLOGY
ATLANTA, GEORGIA 30332

FATIGUE CRACK PROPAGATION OF METASTABLE BETA TITANIUM-VANADIUM ALLOYS

S. B. Chakrabortty and E. A. Starke, Jr.
Fracture and Fatigue Research Laboratory
Georgia Institute of Technology
Atlanta, Georgia 30332

ABSTRACT

The fatigue crack propagation behavior of three titanium-vanadium alloys (24, 28 and 32 wt. % V) which have (tensile) deformation modes ranging from coarse twinning to wavy and planar slip has been measured in laboratory air and correlated with their low cycle fatigue properties and microstructure. The fatigue crack growth rate of alloys with similar microstructures but different deformation modes, and of alloys with similar deformation modes but different microstructures have been compared. Increasing the deformation barrier mean free path and improving low cycle fatigue properties has been observed to reduce the fatigue crack growth rate at low and intermediate ΔK levels. The fatigue crack growth data have been compared with that calculated from equations which use microstructure and low cycle fatigue parameters. The predictive capability of these equations which contain only measurable parameters has been found to be quite adequate.

GLOSSARY

a = total crack length

b = fatigue strength exponent

c = Coffin-Manson exponent

COD = crack opening displacement at maximum load

da = change in crack length

dN = change in number of cycles

E = modulus of elasticity

H = half height of specimen

k' = cyclic strain hardening coefficient $\{\Delta\sigma = k' (\Delta\varepsilon_p)^{n'}\}$

K = stress intensity level

n = monotonic strain hardening exponent

n' = cyclic strain hardening exponent

N = total number of cycles

W = width of sample

$\Delta\varepsilon_p$ = plastic strain amplitude

ΔK = stress intensity range

$\Delta\sigma$ = applied stress amplitude

ε_f = monotonic fracture strain

ε_f' = fatigue ductility coefficient

ε_y' = cyclic yield strain

λ = mean free path between major deformation barriers

ρ^* = microstructural parameter from the Majumdar and Morrow equation

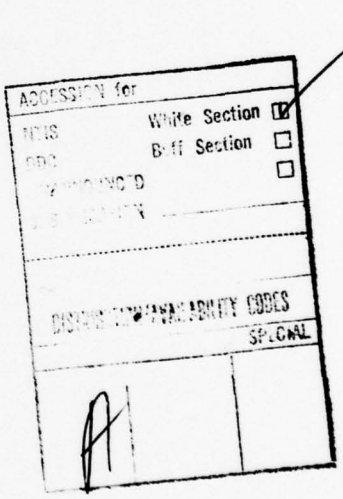

ρ_i' = microstructural deformation zone size of the i^{th} order

σ_f' = monotonic strength coefficient

σ_{ys} = montonic yield strength

σ'_{ys} = cyclic yield strength

INTRODUCTION

Various theories have been proposed to explain the fatigue crack propagation (FCP) behavior of metals and alloys[1-15]. Most theories describe FCP with equations having adjustable constants which can be obtained only after the FCP study is completed. Therefore, they do not suggest those metallurgical variables that can be changed to improve FCP resistance. Two equations have recently been developed which predict FCP behavior using material properties and no adjustable constants.

Liu and Iino[7] assume that cummulative damage by strain cycling causes cracks to propagate. The material of a finite element in the reverse plastic zone (RPZ) ahead of the crack-tip experiences cyclic strain of increasing magnitude as the crack propagates toward it. Each cycle produces damage to the material and if one used Miner's[16] cumulative damage law and Coffin-Manson's[17-18] cyclic life-strain response law an expression for fatigue crack growth rate (FCGR) per cycle may be derived. Majumdar and Morrow[6] and recently Chakrabortty[15] have proposed some modifications of the Liu and Iino approach to incorporate a microstructural parameter along with low cycle fatigue (LCF) parameters to predict the FCGR. The microstructural parameter is taken in terms of the mean free path (λ) between major deformation barriers and the LCF parameters are the cyclic ductility and the cyclic flow stress.

This work concerns the study of the effect of changes in the microstructure and LCF properties of metastable β Ti-V alloys on their FCGR in laboratory air. Starke and coworkers[19-22] have shown that the

deformation modes, microstructure and LCF properties of these alloys may be varied substantially by varying the vanadium content and aging time and temperature. Three alloys (24% V, 28% V and 32% V) were chosen for this study. In the as-quenched condition the deformation behavior changes from coarse twinning and fine wavy slip for the 24% V alloy to coarse planar slip for the 32% V alloy. When the 24% V alloy is aged to contain small amounts (up to $\sim$ 5%) of α precipitates the deformation mode and LCF behavior remains almost unchanged. However, with further aging the volume fraction of α increases, and the deformation behavior changes to planar slip. During LCF the as-quenched and low-α 24% V alloys deform initially by twinning and subsequently by wavy multiple slip. The as-quenched 32% V usually deforms by planar slip. The behavior of the as-quenched 28% V alloy is somewhat intermediate between the 24% V and 32% V alloys. By using the Ti-V system, one may independently vary microstructure or deformation mode by suitably varying the heat treatment and/or composition. This allows an examination of the effect of each parameter on the FCP resistance.

EXPERIMENTAL

Three Ti-V alloys containing 24, 28, and 32 wt.% vanadium were prepared by Titanium Metals Corporation (Henderson, Nevada), where 14 cm diameter ingots were hot forged and cross rolled to produce 15X15X0.8 cm plates having a random texture. The chemical analysis and grain intercept lengths of these materials are shown in Table 1. Samples from the as-received plates were solutionized at 850°C in dry argon and quenched in iced brine. Some samples were aged to produce the desired microstructure and deformation mode (Table 1). Compact

tension[23] samples with H/W of 0.486 and W = 44.5 mm were used to measure the fatigue crack growth rate (FCGR). FCGR measurements were performed on a servohydraulic closed-loop MTS testing machine using tension-tension loading with a maximum/minimum load ratio (R) of 0.1 at a frequency of 10 Hz. The tests were carried out in laboratory air with a relative humidity of 27-30% and a temperature of 23-25°C. The crack length was measured on the polished surface of the specimen using a Gaertner travelling microscope within ± 0.01 mm. The microstructure, deformation and fracture behavior was characterized by x-ray diffraction, and optical and electron microscopy

RESULTS

General Crack Growth Behavior: The measured FCGR versus ΔK curves for all the materials tested in our studies were very similar in character. At low ΔK the FCGR increases slowly with ΔK (AB in Figure 1). At intermediate ΔK accelerated crack growth occurs and there is a sharp increase in da/dn with a small increase in ΔK (BC in Figure 1), after which the FCGR again increases slowly (CD in Figure 1). The fractographic features for all alloys corresponding to this FCGR behavior at various ΔK ranges may be described as follows:

(1) MULTIFACETED crack growth at low rates ($da/dn < 1X10^{-8}$m/cycle). The fracture surface appears to have small ill-defined cleavage facets which are considerably smaller than the grain size. The fracture surface is extremely rough in appearance and crack branching is prevalent. Even though the growth is crystallographic, no single path is preferred. This coincides with the range AB in Figure 1. The typical multifaceted fracture surface features are shown in Figure 2.

(2) FACETED crack growth at intermediate rates ($\sim 1X10^{-8}$ m/cycle < da/dn < $\sim 2.5X10^{-7}$ m/cycle). The fracture surface is composed of large facets each of which usually covers one whole grain. The appearance is similar to that observed on other metallic samples fatigued in air[24]. Facets are shiny and have many river pattern markings. Fracture planes of one system are preferred for each grain resulting in the familiar "stair case" morphology. Fatigue striations become visible on these surfaces above a FCGR of $\sim$ 0.02 μm/cycle. The striation spacing is approximately equal to the crack growth distance per cycle. The transition from multifaceted to faceted growth appears to be associated with an accelerated crack growth rate behavior (region BC of Figure 1). Faceting persists approximately up to point D after which a slow transition to noncrystallographic crack growth occurs. The typical faceted fracture surface features are shown in Figure 3. Transmission electron diffraction studies showed that the facet planes are close to either {100} or {112}.

(3) NONCRYSTALLOGRAPHIC crack growth at higher rates (da/dn > $\sim 2.5X10^{-7}$ m/cycle). The fracture surface is more or less flat, is perpendicular to the stress axis, and is composed of fatigue striations and microvoids (at higher FCGR). The crack path appears to be noncrystallographic. The typical noncrystallographic fracture surface features are shown in Figure 4.

Fracture features are seldom completely of one type. Mixed mode of fracture is present to a different extent in different cases. For the 24A alloy the fracture features indicate some multifaceted growth even

for growth rates as high as 1 μm/cycle. Fatigue striations are never observed on such features which appear to be cleavage. However, fatigue striations are observed on faceted areas, perhaps indicating a fracture involving plastic flow. The crack path appears transcrystalline in most cases. Some intergranular cracking is sometimes observed. Frequent crack branching is observed, especially at lower ΔK ranges (Figure 2).

Comparison of Crack Growth Behavior of Alloys: The materials tested in our studies may be divided into three groups as shown in Table 1. Fatigue crack growth behavior of each of these groups is discussed below:

GROUP 1. This group has three as-quenched alloys with changing vanadium content (i.e., 24A, 28A and 32A), with somewhat similar microstructures, and different deformation modes. 24A deforms primarily by coarse twinning and wavy slip, 28A deforms by wavy slip and 32A deforms by planar slip. At low ΔK ranges, 32A has the lowest FCGR and 24A has the highest (Figure 5). However, the opposite seems to be true at an intermediate range. The accelerated crack growth behavior at this range is maximum for 32A and minimum for 24A. Similar anomalous accelerated growth behavior has been found in Ti-6-4[25] and Al-7Mg[26] alloys. Our results show that the extent of accelerated growth and the associated faceting is increased by increasing the propensity of coarse slip by increasing the vanadium content (24A << 28A < 32A).

24A alloys deform by coarse twinning during tensile and low-cycle and high-cycle fatigue tests. However, no deformation twins were observed by optical microscopy during the FCP test when the ΔK was below $\sim$ 10 MPa$\sqrt{m}$. Perhaps, the deformation at the crack tip is restricted

to a narrow area at such low ΔK and the formation of coarse twins is not possible. Consequently, the material at the crack-tip deforms by wavy slip. At higher ΔK, deformation twins form. When the crack intersects a twin it sometimes follows the twin boundary for a short distance and again becomes transgranular. However, twin boundaries do not appear to play a major role in FCP.

GROUP 2. This group consists of three different heat-treated conditions of the Ti-24 V alloy. All conditions deform primarily by twinning and wavy slip. The propensity of twinning decreases with increasing amount of alpha precipitation. Figure 6 shows the da/dn versus ΔK curves for these materials. Increasing the volume fraction of α precipitates in the β matrix increases the FCGR. From the fractographic examination of areas around α precipitates, it appears that these particles do not embrittle the material. Ductile fatigue striations are observed in and around the precipitate/matrix interface and the spacing appears to be the same as that observed away from the precipitates (Figure 7). The fracture features for this alloy group were very similar for the same da/dN; however, they were quite different for the same ΔK, as seen by the comparison of 24A and 24C in Figure 8. More extensive deformation occurs for 24C than for 24A at similar ΔK values. It appears that the effect of increasing the amount of precipitate is to increase the extent of crack-tip plasticity for a given ΔK and therefore to increase the FCGR. At high ΔK when non-crystallographic growth occurs, the FCGR is more or less similar for all of the three structures.

GROUP 3. This group has two materials which deform by planar slip. 32A is an all-beta-phase alloy, and 24D has been heat treated to produce a large amount of alpha precipitates in the beta matrix. As for Group 2, the effect of the precipitates is to increase the FCGR (Figure 9) for the crystallographic growth region. Both 32A and 24D deform by coarse planar slip and consequently show an accelerated crack growth behavior for intermediate ΔK.

Comparison Between Calculated and Experimental FCGR: To our knowledge only two equations are available to calculate the FCGR from LCF data and microstructural parameters without the use of any adjustable constants. The equation proposed by Majumdar and Morrow[6] is

$$\frac{da}{dN} = \frac{-2(b+c)}{b+c+1}\left[\frac{\sigma'_y}{4(1+n')\sigma'_f\varepsilon'_f}\right]^{\frac{-1}{b+c}}\left\{\left[1+\frac{2\rho^*}{COD}\right]^{\frac{b+c+1}{b+c}} - \left[4(1+n')\varepsilon'_y\right]^{-\frac{b+c+1}{b+c}}\right\}\frac{\varepsilon'_y\Delta K^2}{\pi\,\sigma'^2_y} \quad (1)$$

Chakrabortty[15] related FCGR to ΔK and low cycle fatigue parameter with the following equation:

$$\frac{da}{dn} = 2\sum_{n=1}^{\infty}\rho'_n\left(\frac{\Delta\varepsilon_{pn}}{2\varepsilon'_f}\right)^{-\frac{1}{c}} \quad (2)$$

where, $\Delta\varepsilon_{p_n} = \int_{x=r_{n-1}}^{x=r_n} \Delta\bar{\varepsilon}_p\, x^{\frac{1}{2}}dx \Big/ \int_{x=r_{n-1}}^{x=r_n} x^{\frac{1}{2}}dx$

$$x = \frac{\Delta K^2}{(1+n')\pi E k'} \cdot \frac{1}{(\Delta\bar{\varepsilon}_p)^{n'+1+\frac{k'}{E}}(\Delta\bar{\varepsilon}_p)^{2n'}}$$

$$r_n = r_o + \sum_{i=1}^{n}\rho_i'$$

and $r_o = \frac{\Delta K^2}{\pi\sigma'_y E}$

The microstructure parameter ρ of equations (1) and (2) is proportional to λ. The results of calculations using equations (1) and (2) are presented in Figure 10. Calculations were made only for 24A, 24B, and 24C since these have the smallest environmental effect. The results obtained by equation (2) fall well within the expected scatter band of the experimental data. The Majumdar and Morrow equation appears to be good only at high ΔK, and at low ΔK values it considerably underestimates the FCGR.

DISCUSSION

Modes of Crack Growth: In order to explain our results we propose that the following three mechanisms of fatigue crack propagation are operative in the stress intensity ranges which correspond to the three fractographic features described.

1. At low ΔK, multifaceted crack growth occurs by decohesion along {110} and/or {112} slip bands or possibly by either {100}, {110}, or {123} cleavage in the cyclic plastic zone ahead of the crack-tip. Cracking may occur simultaneously in numerous areas of the same grain, and depending upon the material all cracks may not be on parallel crystallographic planes. The observed multifaceted appearance results from link-up of numerous cracks. Other authors have proposed a similar model to explain the FCP behavior of some alloys at low ΔK.[27-29]
2. Faceting behavior observed at intermediate ΔK is due to shearing along coarse slip band(s) at the crack-tip. The coarse slip bands form ahead of the crack-tip during cyclic deformation and the crack extends due to shearing off the coarse slip band(s) during tensile

loading. However, depending on the environment and number of active slip bands some "rewelding" of the crack may occur during compression. This mode of crack propagation should be enhanced for a material with coarse slip character and by any environment which would inhibit rewelding. The fracture plane will depend on the number and type of operative slip systems at the crack-tip, and within one grain will be determined by the stress-axis-grain orientation relationship. The resulting faceted appearance is composed of long planar surfaces with lengths equal to the grain size and parallel to the crack growth direction, having the stair case morphology of Figure 3. Other authors have proposed models explaining the detailed crystallographic aspects of this mode of growth.[30-32]

3. At high ΔK, the noncrystallographic growth is due to a crack-tip stretching mechanism. The crack tip moves by inward contraction of the material during tensile deformation until blunting occurs. The crack resharpens during compression. The extent of crack growth per cycle should depend mainly upon the cyclic flow stress of the material. The geometry of crack-tip stretching dictates that the fracture plane be perpendicular to the loading direction. Therefore, the observed noncrystallographic fractographic appearance with ductile fatigue striations is expected. A similar mechanism has been proposed previously for high-stress fatigue.[33-35]

The operating fracture mode depends upon the deformation behavior of the material, the environment and the stress intensity range. The require-

ments for faceting are the formation of coarse slip and lack of complete reweldability of the freshly formed "crack" during the compressive cycle. Therefore, there may be a critical value of stress intensity range (ΔK_f), below which faceting is not possible. Below ΔK_f coarse slip may not occur; or even if it does occur the crack extension in the tensile stroke may be sufficiently small for rewelding to be complete during compression. The value of ΔK_f should decrease as the environment becomes aggressive, although faceting may occur even without an aggressive environment. A suitable environment only reduces the energy necessary for such growth by reducing crack-tip reweldability and/or by increasing cyclic coarse slip. The probability of faceting fracture will also be increased when the material has greater propensity of coarse slip. Below ΔK_f faceting is reduced because the decohesion mechanism requires less energy. As ΔK increases the probability of multiple slip increases and coarse planar slip decreses. Consequently, there is also a ΔK above which faceting diminishes. Here the environment becomes inconsequential becasue the crack-tip blunts due to plasticity effects. Figure 11 is a schematic illustration of FCGR corresponding to each mode of growth for a Ti-V alloy.

The proposed modes of crack growth explain the observed fractographic features. The accelerated phenomenon associated with the onset of faceting is schematically illustrated in Figure 11. Our results show that accelerated growth and faceting increases when the propensity of coarse slip is increased either by increasing the vanadium content (24A << 28A < 32A) or by varying the heat treatment (24A ≤ 24B ≤ 24C < 24D). Furthermore, as expected from the proposed modes, our results

indicate that there is a ΔK_f for faceting, which appears to decrease with increasing propensity of coarse slip. Recent results[36] have shown that ΔK_f decreases and the probability of faceting increases in more aggressive environments than used in this study. The coarse slip-fracture model proposed by Neumann,[31] predicts {001} and {112} fracture planes for alloys having {110} <111> and {112} <111> operative slip systems. This prediction is consistent with our results.

Correlation Between Calculated and Measured FCGR: Equation (1) proposed by Majumdar and Morrow,[6] and Equation (2) by Chakrabortty[15] assume that the material ahead of the crack-tip undergoes cyclic plastic deformation, and crack extension occurs due to exhaustion of the fatigue ductility of the material. The Chakrabortty model[15] estimates the cyclic plastic strain by dividing the cyclic plastic zones into elements of size ρ_i and assuming that the cyclic deformation is more or less uniform within these elements. According to this model the element nearest to the crack-tip contributes most to the FCGR at low ΔK. Majumdar and Morrow s model[6], on the other hand, ignores the contribution of this element because continuun mechanics and bulk properties are not applicable with such a small zone. This explains why the calculated FCGR values from the Majumdar and Morrow equation falls orders of magnitude below the experimental data for the lower ΔK range. The Chakrabortty equation appears to predict the FCGR values more accurately over all ranges of ΔK (Figure 10). However at low ΔK, the experimental curves are somewhat below the predicted curves. This is expected due to crack branching since crack branching reduces the effective ΔK and the measured crack growth rate (if the projected crack-length is used).

The crack growth data and fractographic features support the Chakrabortty model.[15] According to the model the FCGR increases as one decreases the cyclic flow stress, the cyclic ductility and the mean free path (λ) between the major deformation barriers. This predicts that the group 1, 2 and 3 alloys should be ranked 24A, 28A, 32A; 24B, 24A; and 24D, 32A, respectively in order of reducing FCGR. The experimental data agree well with this prediction with one exception; for the faceted growth region for Group 1 alloys the order is reversed. This is possibly a result of a different environmental effect for the different alloys. 32A, which has the highest propensity of coarse slip, should have the largest environmental effect. The value of λ is decreased in Group 2 alloys by heat treatments which produce α particles within the β matrix. The cyclic flow stress and ductility remains more or less unchanged. According to the model, a reduction in λ causes an increase in cyclic plastic deformation in the element just ahead of the crack-tip and this should increase the FCGR as observed in our experiments, Figure 6. Furthermore, the fractographic features seem to indicate that for the same ΔK, the cyclic deformation is largest for 24C which has the lowest value for λ. On the other hand, the deformation appears very similar for the same da/dn, Figure 8. A similar behavior was observed for Group 3 alloys. The model also predicts that when ΔK is large, the crack growth rate becomes less dependent on λ and the FCP should become structure insensitive. The data again supports this prediction -- 24A, 24B and 24C which have same fatigue flow stress and ductility but different λ have similar crack growth rate values at high ΔK.

Both the Majumdar and Morrow and Chakrabortty equations predict that a decrease in λ will increase the FCGR unless the fatigue flow stress and/or fatigue ductility is improved drastically.[15] Therefore, these equations propose that a decrease in λ, which is usually benefical for the strength, ductility, LCF and HCF properties, may be detrimental for FCP resistance. Experimental results on various alloy systems support this prediction.[24]

SUMMARY

Three different modes of fatigue crack growth have been observed for the metastable beta titanium-vanadium alloys tested. They are: (1) The fracture surface is composed of small cleavage-like areas at low ΔK and is assumed to be a product of decohesion along slip planes or cleavage planes as a result of fatigue cycling. (2) At intermediate ΔK faceting is observed and is assumed to occur by a cyclic coarse slip mechanism where crack extension is due to irreversable shearing off in coarse slip bands. This mode of crack growth appears to be sensitive to environment. (3) At high ΔK the crack surface has a striated non-crystallographic appearance. Here, it is assumed that the crack grows by the inward contraction of the crack-tip due to stretching of the material at the tip. The faceting mechanism appears to be enhanced by coarse slip and aggressive environments. Transition from multifaceted to faceted growth is always associated with an accelerated crack growth rate behavior.

Comparison of some of the experimental data with those calculated from the equations of Chakrabortty[15] and Majumdar and Morrow[6] shows good correlation. Fractographic features also seem to support the model proposed by Chakrabortty.[15] It is observed that where cyclic flow

stress and ductility is kept nearly constant, the FCGR value increases when the mean free path between the major deformation barrier (λ) is decreased. Also when λ is kept nearly constant the FCGR is increased when the cyclic flow stress and/or ductility is decreased. When the environment has a large effect, the material with higher propensity of coarse slip shows a very high crack growth rate regardless of the values of cyclic ductility, flow stress, and λ.

ACKNOWLEDGEMENTS

The authors would like to acknowledge the help of Mr. Eui Whee Lee with the experimental measurements. This research was supported by the Office of Naval Research under Contract N00014-75-C-0349, Dr. Bruce A. McDonald, Contract Monitor. The United States Government is authorized to reproduce and distribute reprints for Government purposes notwithstanding any copyright notation hereon.

REFERENCES

1. J. Weertman, Int. J. Fract. 9, 125 (1973).
2. T. Mura and C. T. Lin, Int. J. Fract. 20, 284 (1974).
3. J. R. Rice, Fatigue Crack Propagation, ASTM STP No. 415, 247 (1967).
4. G. P. Cherepanov and H. Halmanov, Eng. Fract. Mech. 4, 219 (1972).
5. P. E. Irving and L. N. McCartney, Metal Sciences, 11, 351 (1977).
6. S. Majumdar and J. Morrow, Fracture Toughness and Slow-Stable Cracking, ASTM STP No. 559, 159 (1974).
7. H. W. Liu and N. Iino, Proc. 2nd Int. Conf. on Fract., Chapman and Hall, p. 812 (1969).
8. S. D. Antolovich, A. Saxena and G. R. Chanani, Eng. Frac. Mech. 7, 649 (1975).
9. F. A. McClintock, ASTM STP No. 415 (1967). Discussion to article by C. Laird, p. 170.
10. F. A. McClintock, Fracture of Solids, Interscience Publishers, NY, p. 65 (1963).
11. R. W. Larder, Phil. Mag., 17, 71 (1968).
12. H. W. Lin, Trans. ASME 85, 116 (1963).
13. N. E. Frost and J. R. Dixon, Int. J. Fract., 3, 301 (1967).
14. A. J. McEvily, Jr. and T. L. Johnston, Int. J. Fract. Mech., 3, 45 (1967).
15. S. B. Chakrabortty, "Cyclic Ductility, Cyclic Strength and Fatigue Crack Propagation of Metals and Alloys," Technical Report 78-2 Office of Naval Research Contract N00014-75-C-0349, NR 031-750, May 16, 1978.
16. M. A. Miner, J. Appl. Mech. 12A, 159 (1945).
17. L. F. Coffin, Jr., Trans. ASME, 76, 931 (1954).
18. S. S. Manson and H. M. Hirschberg, "Fatigue-An Interdisciplinary Approach" ed. by J. J. Burke, N. L. Reed, and V. Weiss, Syracuse University Press, p. 133 (1964).
19. Fu-Wen Ling, H. J. Rack and E. A. Starke, Jr., Met. Trans., 4, 1671 (1973).
20. Fu-Wen Ling, E. A. Starke, Jr., and B. G. LeFevre, Met. Trans., 5, 179 (1974).

21. H. G. Paris, B. G. LeFevre and E. A. Starke, Jr., Met. Trans., 7A, 273 (1976).

22. S. B. Chakrabortty, T. K. Mukhopadhyay and E. A. Starke, Jr., Acta Met., 26, 909 (1978).

23. ASTM Specification E-399.

24. C. J. Beevers, Fracture, Waterloo, Canada, 1, p. 239 (1977).

25. P. E. Irving and C. J. Beevers, Mat. Sci. and Eng., 14, 229 (1974).

26. F. P. Ford and T. P. Hoar, III Int. Conf. on the Strength of Metals and Alloys, 1, p. 467 (1973).

27. C. D. Beachem and D. A. Meyn, ASTM STP No. 436, 59 (1968).

28. D. J. Duquette and M. Gell, Met. Trans., 2, 1325 (1971).

29. R. W. Hertzberg and W. J. Mills, ASTM STP No. 600, 220 (1976).

30. P. Neumann, Acta Met., 17, 1219 (1969).

31. P. Neumann, Acta. Met., 22, 1155 (1974).

32. G. G. Garrett and J. F. Knott, Acta Met., 23, 841 (1975).

33. D. A. Meyn, Trans. ASM, 61, 42 (1968).

34. C. Laird, ASTM STP No. 415, 131 (1967).

35. C. Laird and G. C. Smith, Phil. Mag., 7, 847 (1962).

36. S. B. Chakrabortty and E. A. Starke, Jr., unpublished work.

TABLE 1: Composition, Heat Treatment, Microstructure and Deformation Modes of Alloys Used for Fatigue Crack Propagation Studies

GROUP	DESIGNATION	COMPOSITION (wt%)	TREATMENT	MICROSTRUCTURE λ*	TENSILE DEFORMATION MODE
1	24A	24V, 0.20_2	AS QUENCHED	$(\beta+\omega)$ $\lambda = 64\mu$	Coarse Twinning + (Wavy Slip)
	28A	28V, 0.20_2		β $\lambda = 97\mu$	Wavy Slip
	32A	32V 0.20_2		β $\lambda = 108\mu$	Coarse Single Slip
2	24A	24V, 0.20_2	AS QUENCHED	$(\beta+\omega)$ $\lambda = 64\mu$	Coarse Twinning + (Wavy Slip)
	24B	24V, 0.20_2	QUENCHED AND AGED	$(\beta+\omega)+\alpha$ $\lambda = 30\ \mu$	
	24C	24V, 0.20_2	QUENCHED AND AGED	$(\beta+\omega)+\alpha$ $\lambda = 12\mu$	
3	24D	24V, 0.20_2	QUENCHED AND AGED	$\beta+\alpha$ $\lambda = 6\mu$	Coarse Single Slip
	32A	32V, 0.20_2	AS QUENCHED	β $\lambda = 108\mu$	

* λ is the mean free path between α particles for alloys with α precipitates, or the grain intercept length for all other alloys.

LIST OF FIGURES

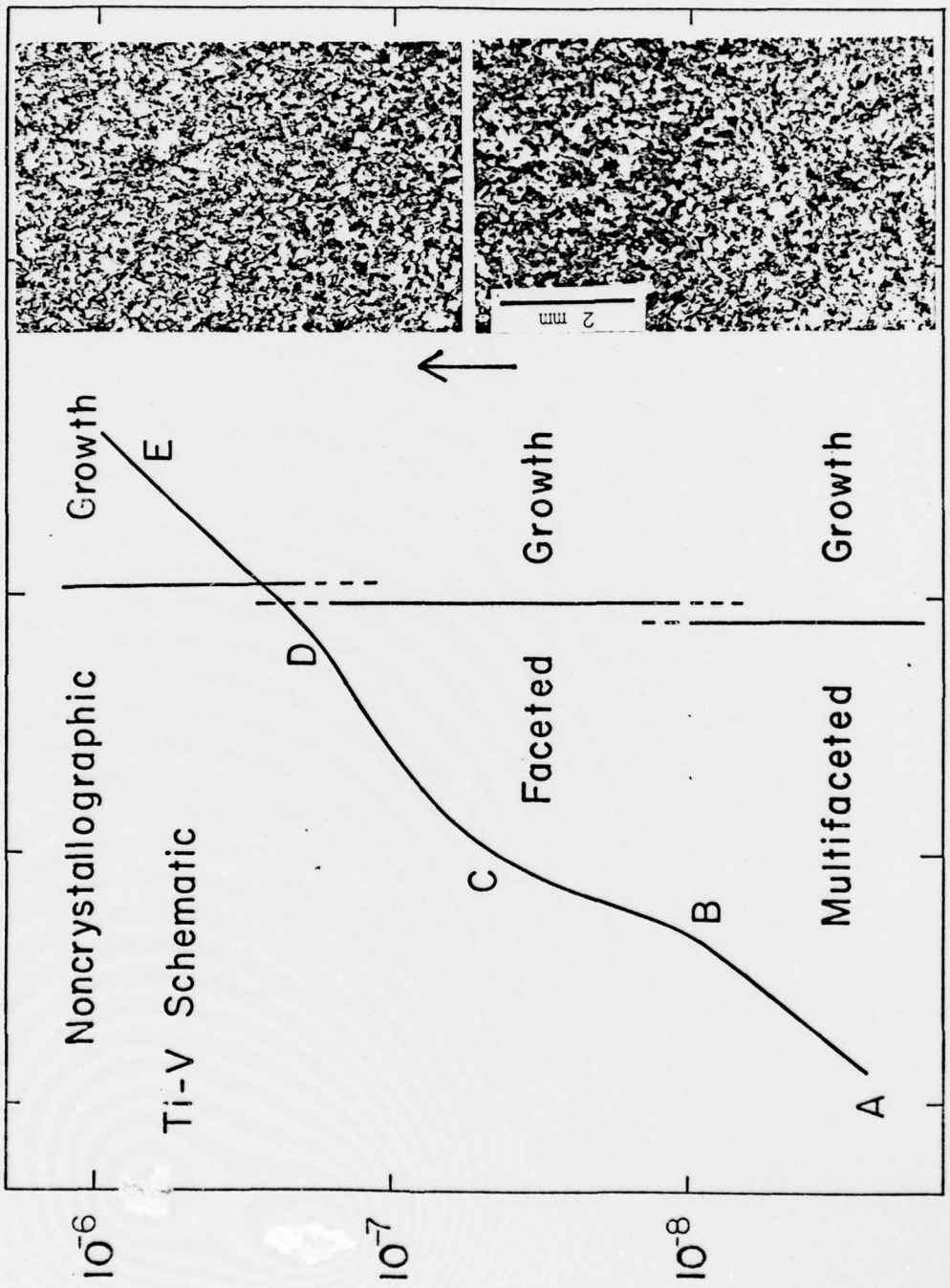

Figure 1. Typical FCGR curve for the Ti-V alloys with the corresponding fracture features.

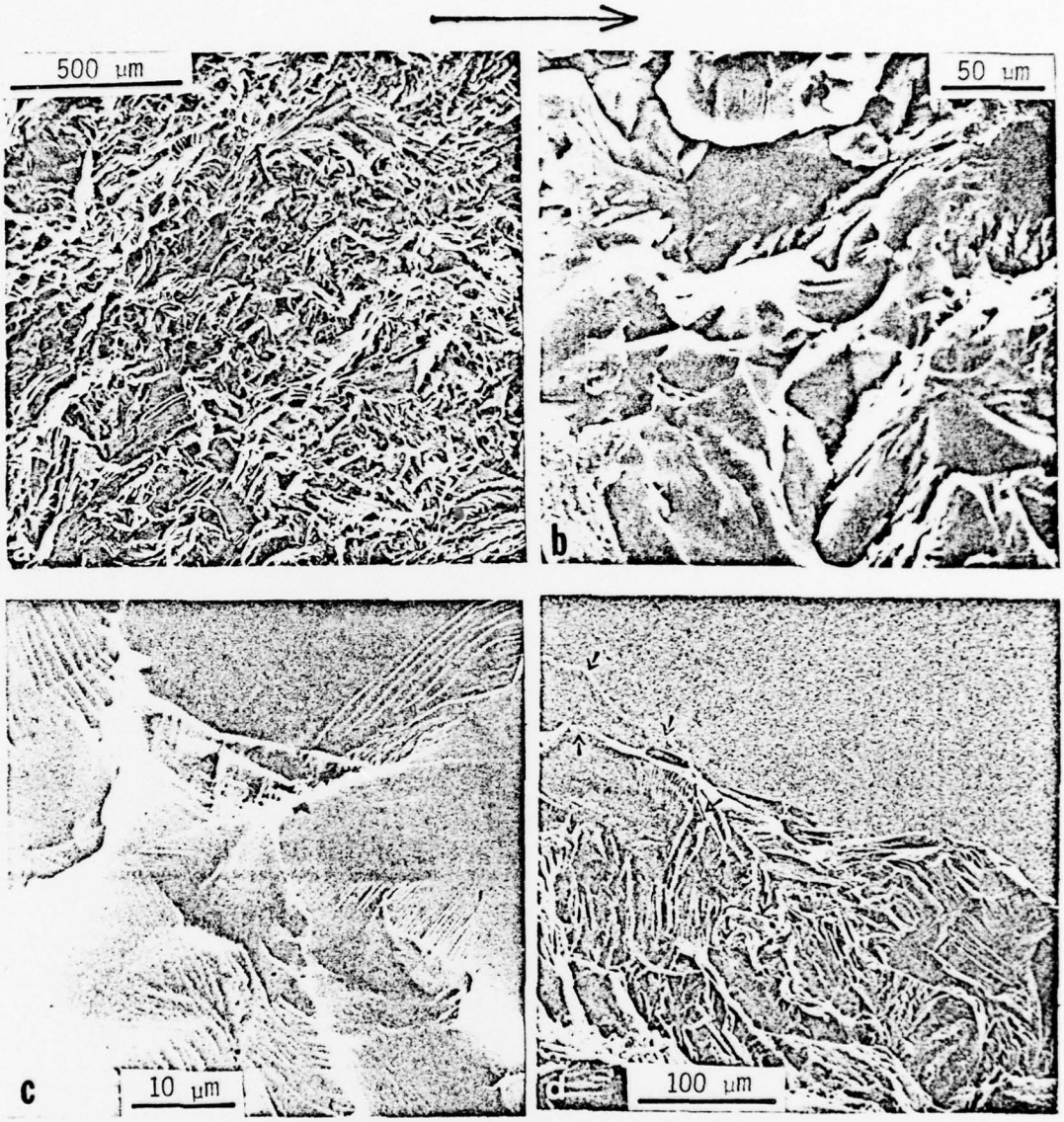

Figure 2. Examples of multifaceted growth features. Ti-28V alloy, as-quenched. $\Delta K \sim 6.5$ MPa$\sqrt{m}$, da/dn $\sim 5 \times 10^{-9}$ m/cycle. Figure 2b is photographed at $\sim 45°$ to both the crack surface and a vertical section. Some secondary cracks are marked with arrows.

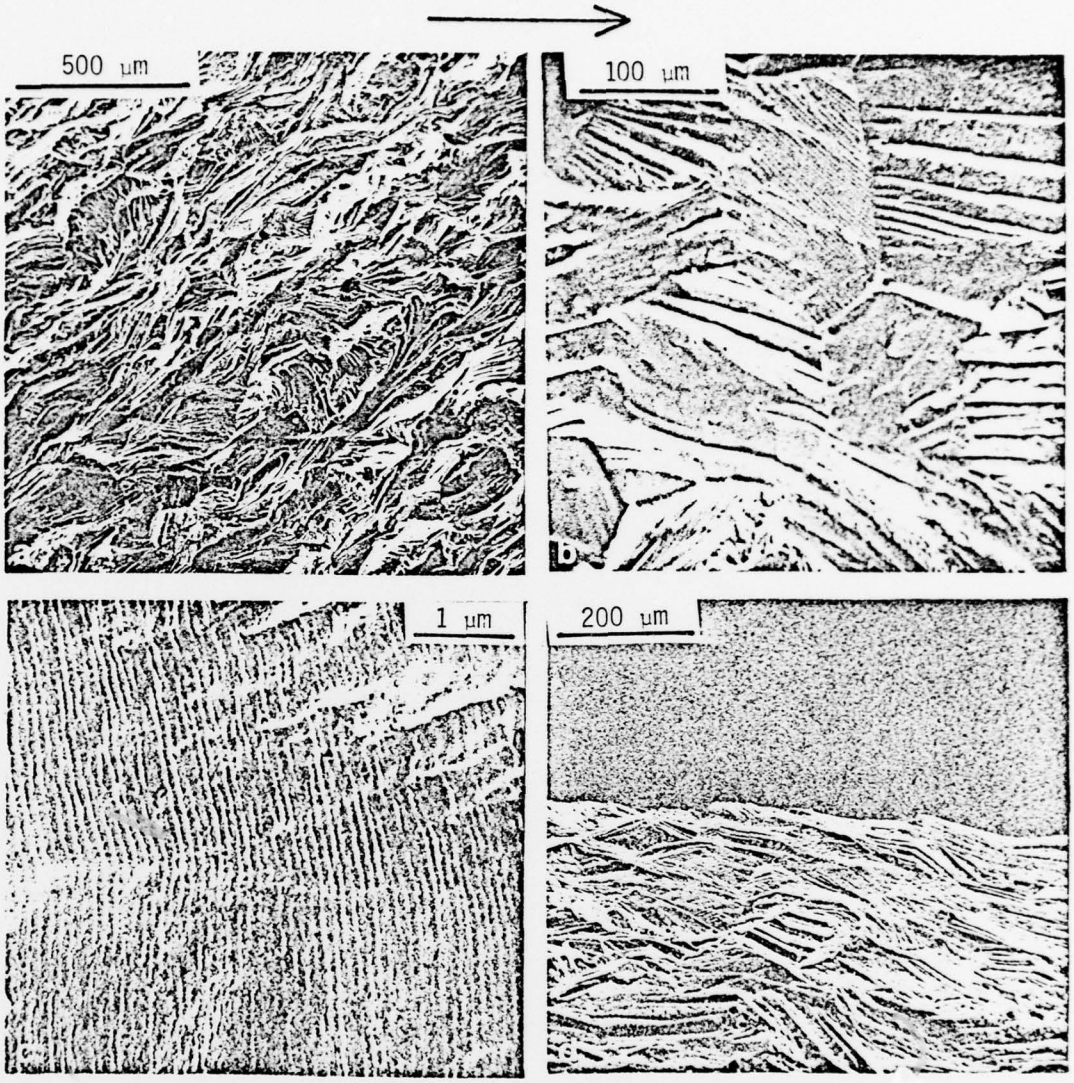

Figure 3. Examples of faceted growth featues. Ti-28V, as-quenched. $\Delta K \sim$ 14.3 MPa$\sqrt{m}$, da/dn $\sim$ 1X10^{-7} m/cycle. Figure 3b is photographed at $\sim$ 45° to both the crack surface and a vertical section.

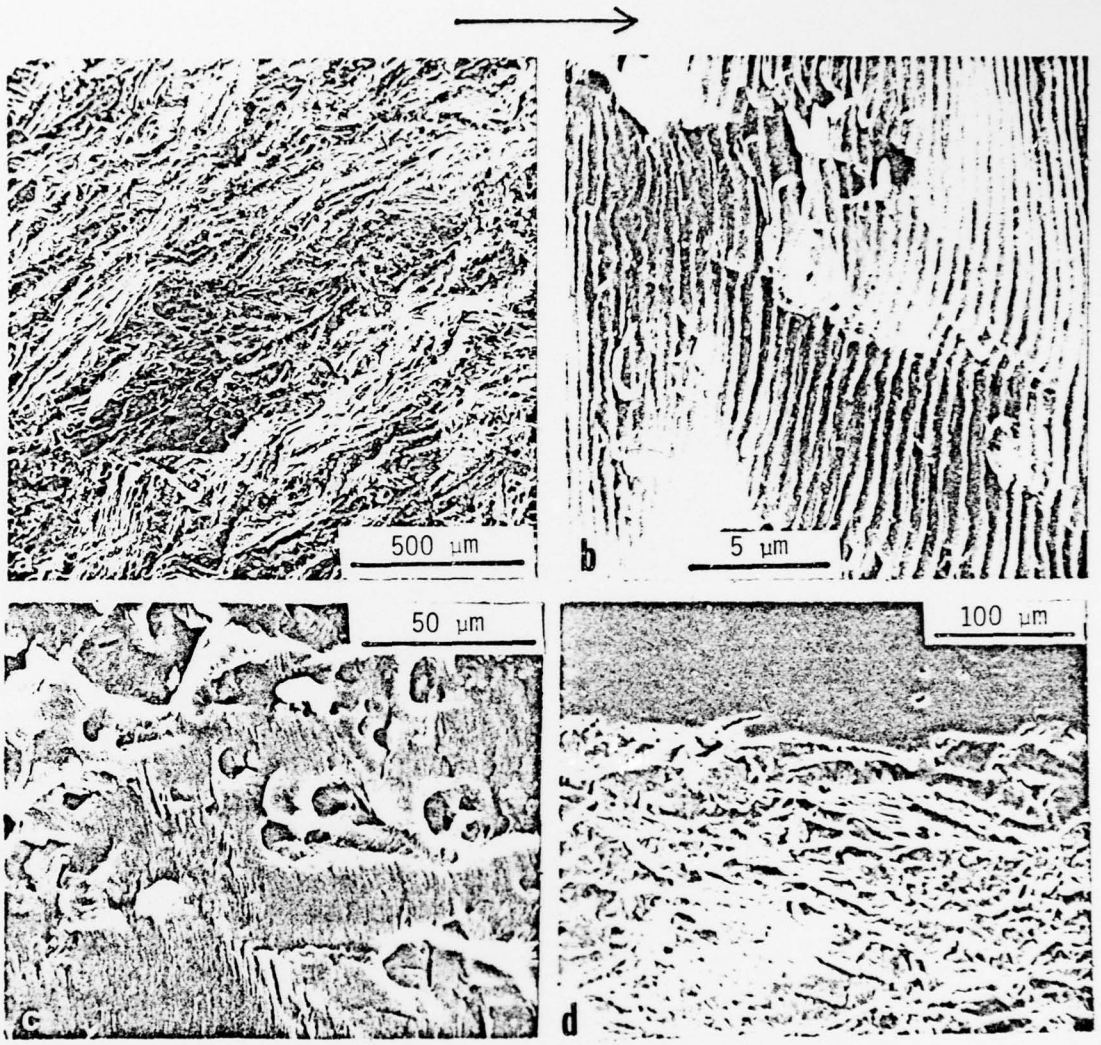

Figure 4. Examples of noncrystallographic growth features. Ti-28V as-quenched. a, b and d- $\Delta K \sim 29$ MPa$\sqrt{m}$, da/dn $\sim 6X10^{-7}$ m/cycle. c.- K $\sim$ 40, da/dn $\sim 1.5X10^{-6}$ m/cycle. Figure 4d is photographed at $\sim$ 45° to both the crack surface and a vertical section.

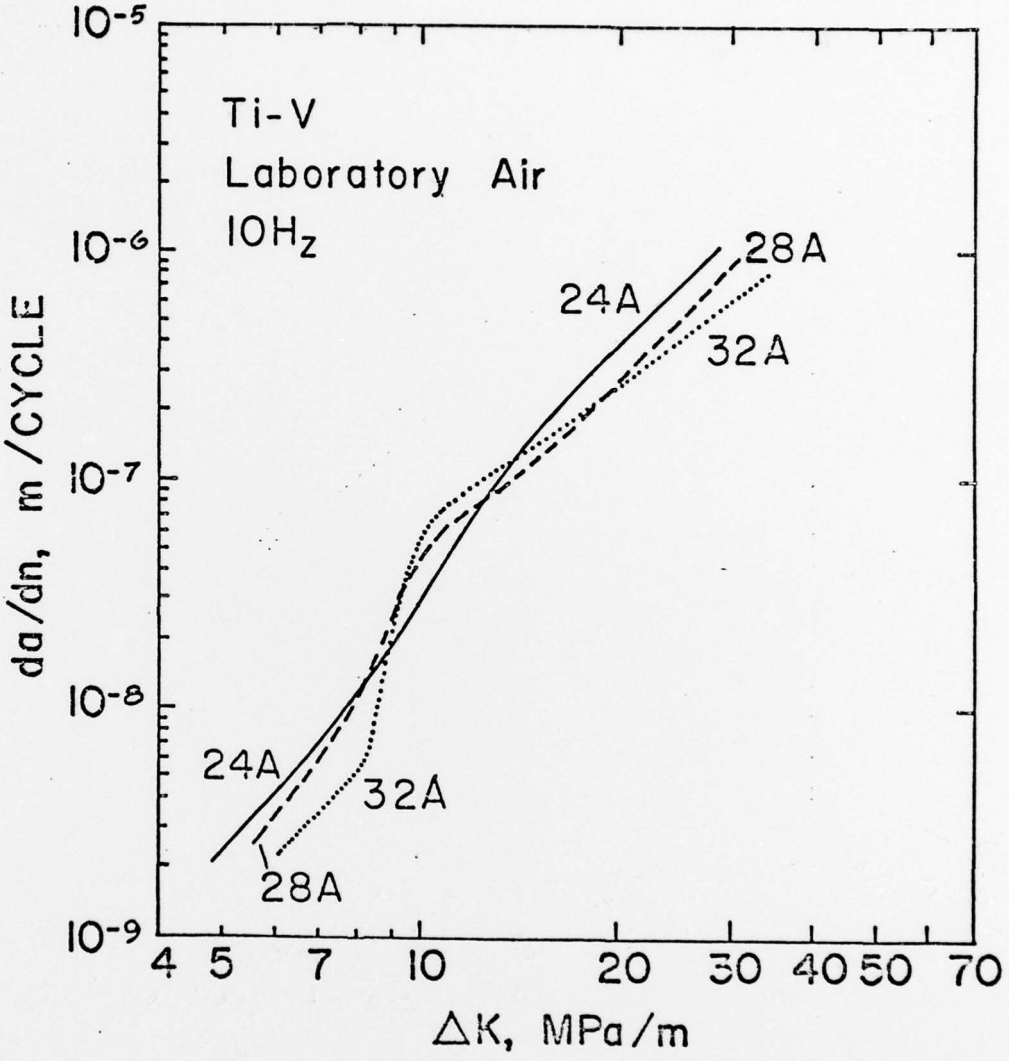

Figure 5. Fatigue crack growth rate versus stress intensity range curves for the Ti-24%V, 28%V and 32%V, as quenched alloys.

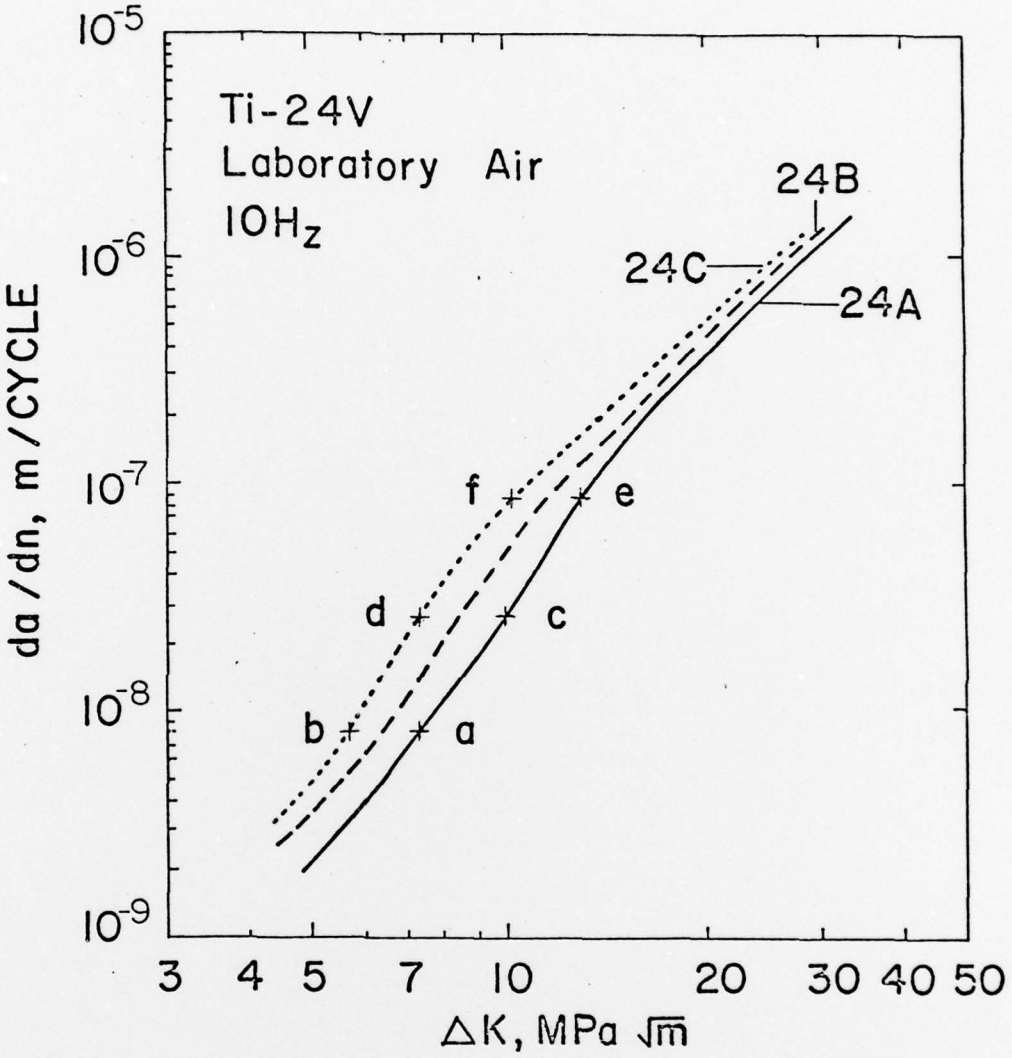

Figure 6. Fatigue crack growth rate versus stress intensity range curves for the Ti-24%V as-quenched and aged alloys.

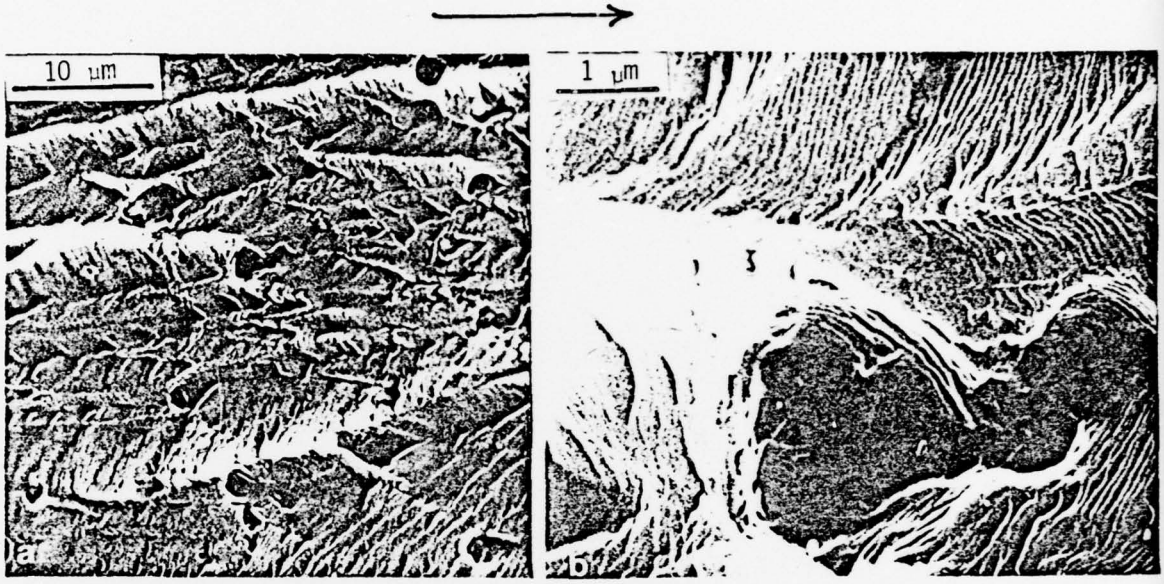

Figure 7. Fractographic features of fatigue crack propagation around the second phase particles of an aged Ti-24%V alloy (24C). $\Delta K \sim 10$ MPA$\sqrt{m}$, da/dn $\sim 8X10^{-8}$ m/cycle.

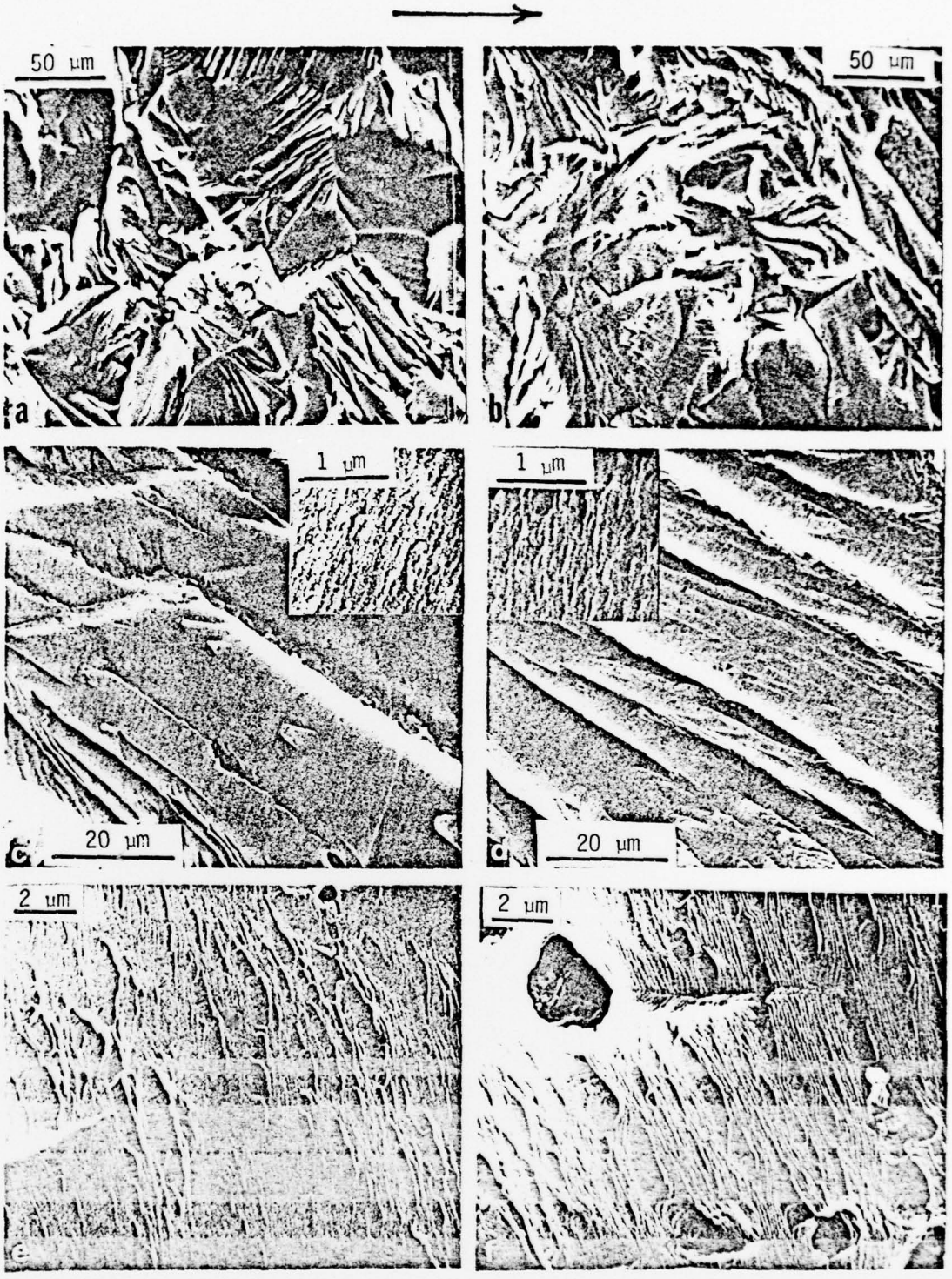

Figure 8. Comparison between the fractographic features of 24A and 24C alloys at various points on the FCGR curves. Figures a, b, c, d, e and f corresponds to the points a, b, c, d, e and f of Figure 6.

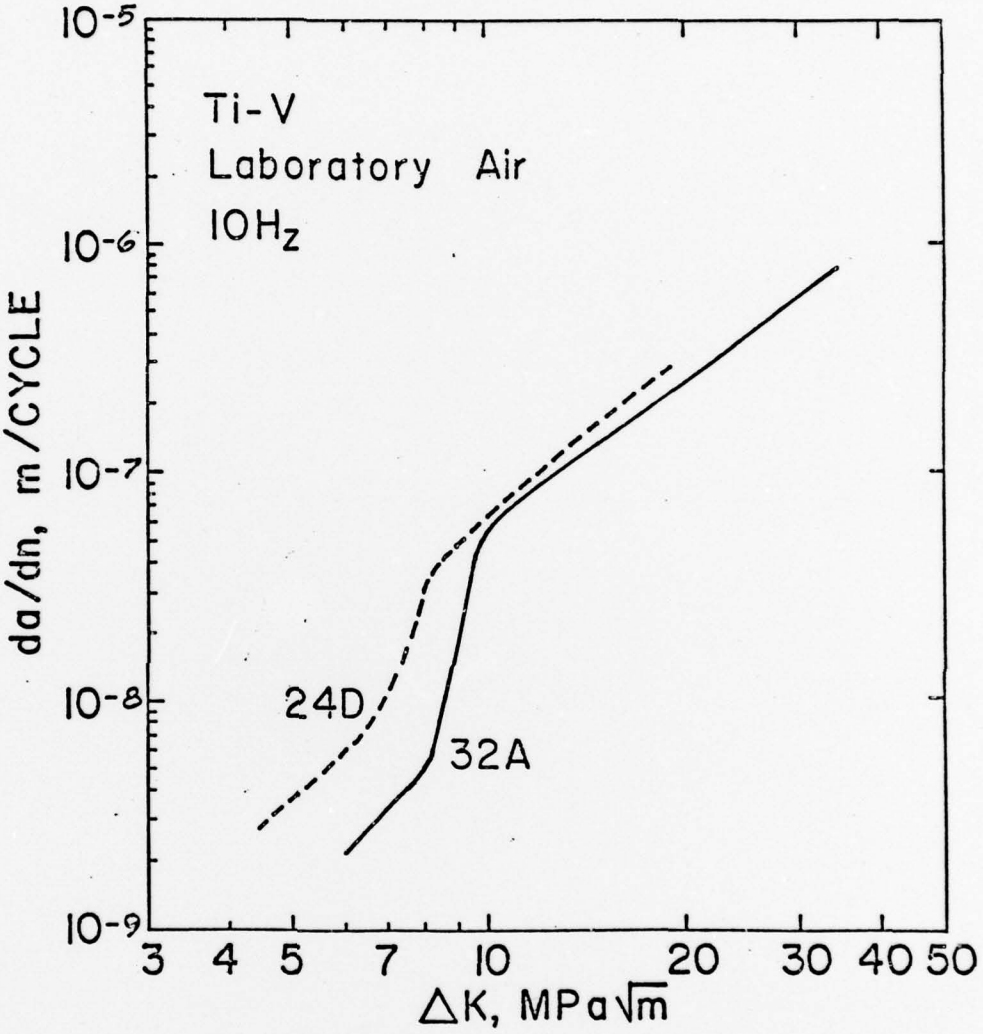

Figure 9. Fatigue crack growth rate versus stress intensity range curves for the 32A and 24D alloys.

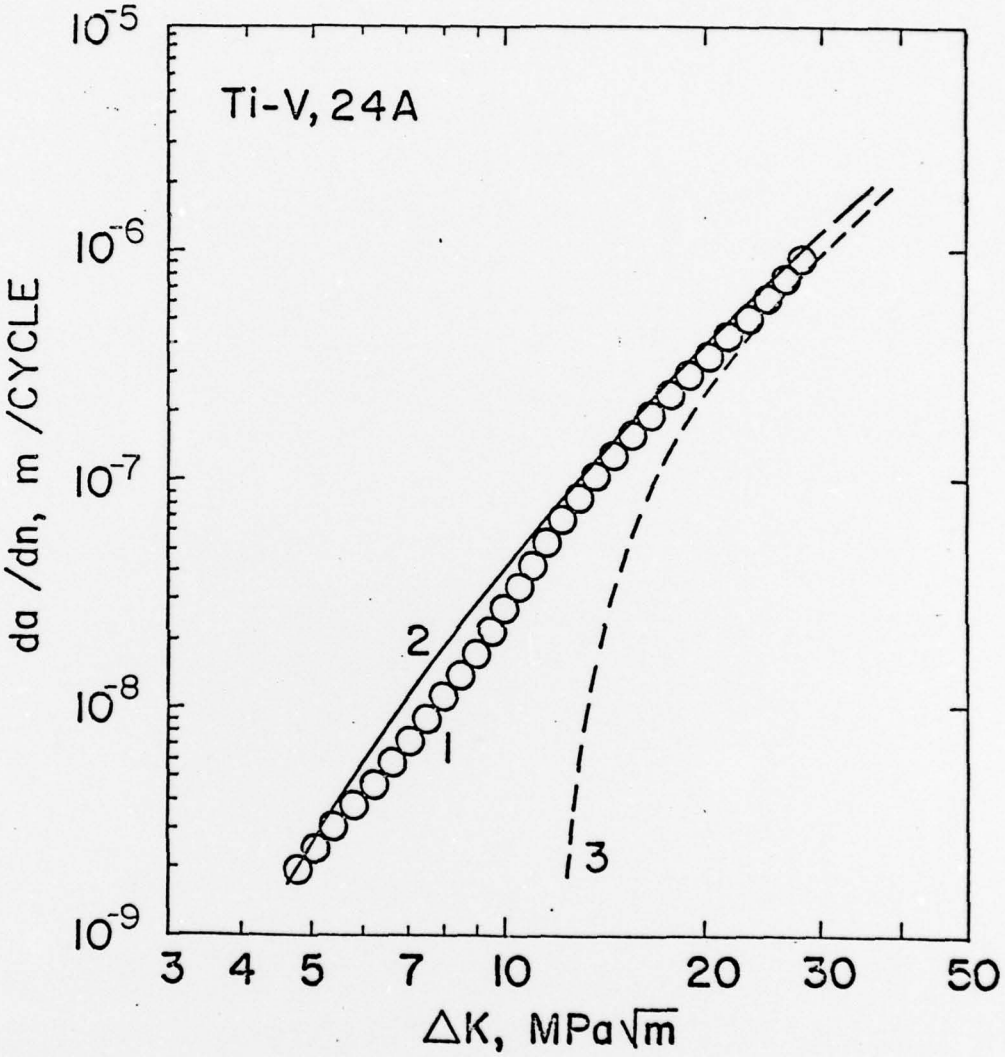

(a)

Figure 10. Comparison between the calculated and experimental fatigue crack growth rate versus stress intensity range curves; (1) Experimental curve, (2) calculated from equation 2, and (3) calculated from equation 1.
(a) for the 24A alloy (λ = 64μ)
(b) for the 24B alloy (λ = 30μ)
(c) for the 24C alloy (λ = 12μ)

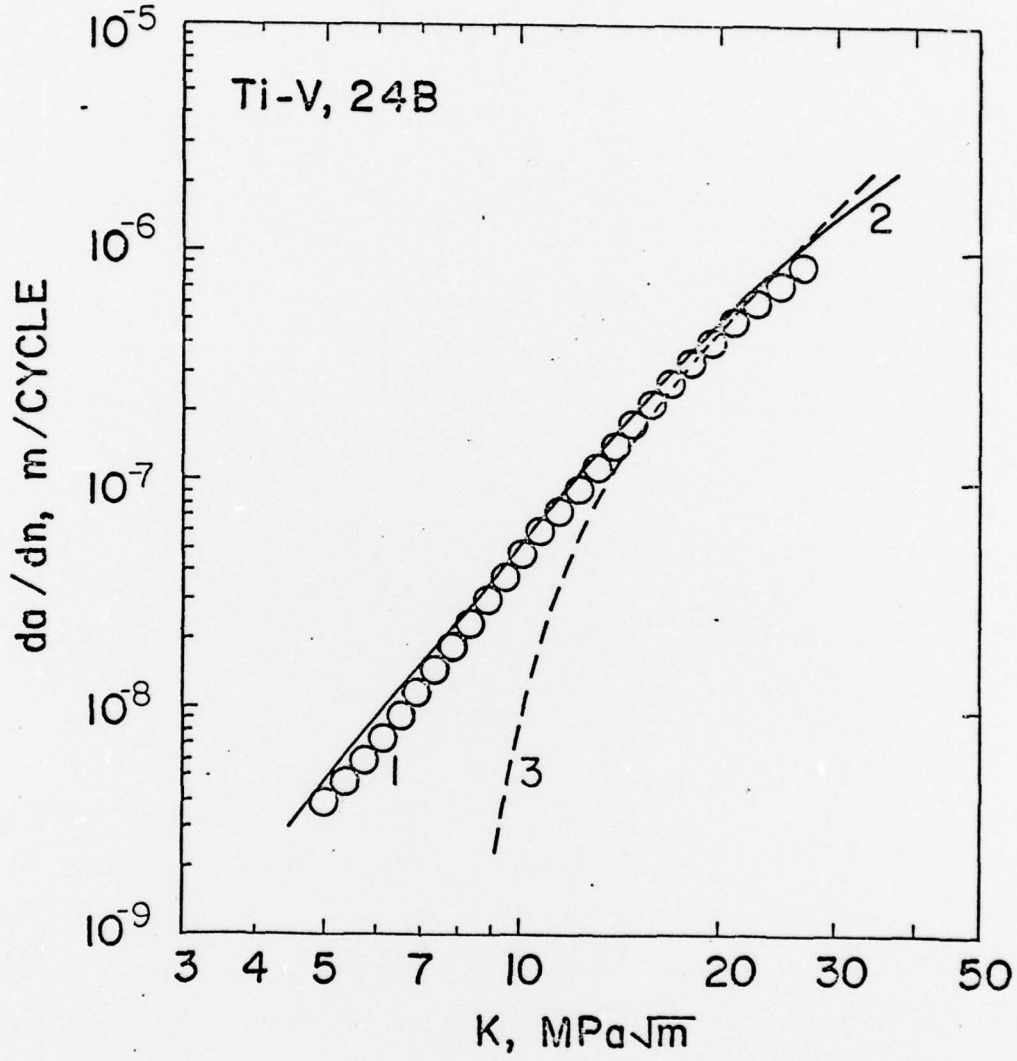
Ti-V, 24B
da/dn, m/CYCLE
10^{-5}
10^{-6}
10^{-7}
10^{-8}
10^{-9}
1
2
3
3 4 5 7 10 20 30 50
K, MPa$\sqrt{m}$

(b)

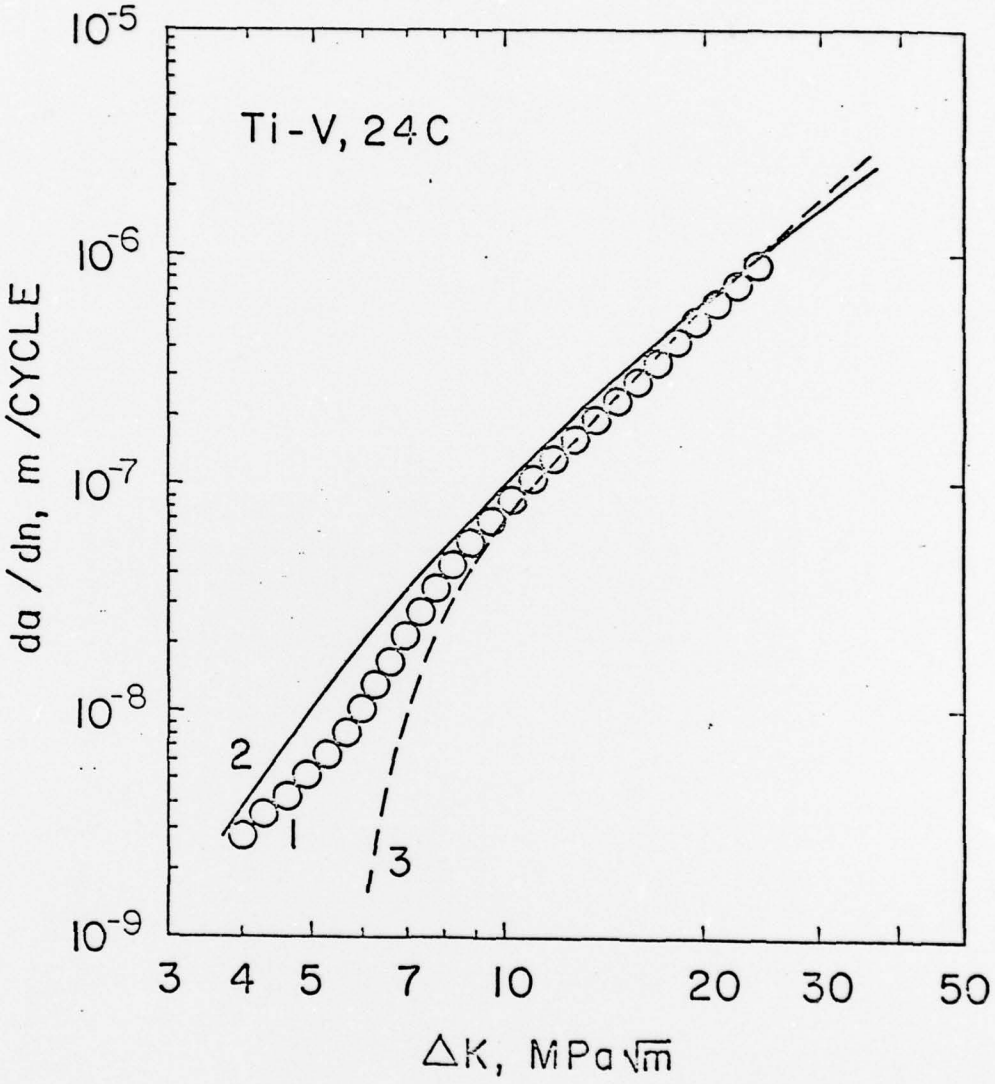
Ti-V, 24C
da/dn, m/CYCLE
ΔK, MPa√m
10^-5
10^-6
10^-7
10^-8
10^-9
3
4
5
7
10
20
30
50
1
2
3

(c)

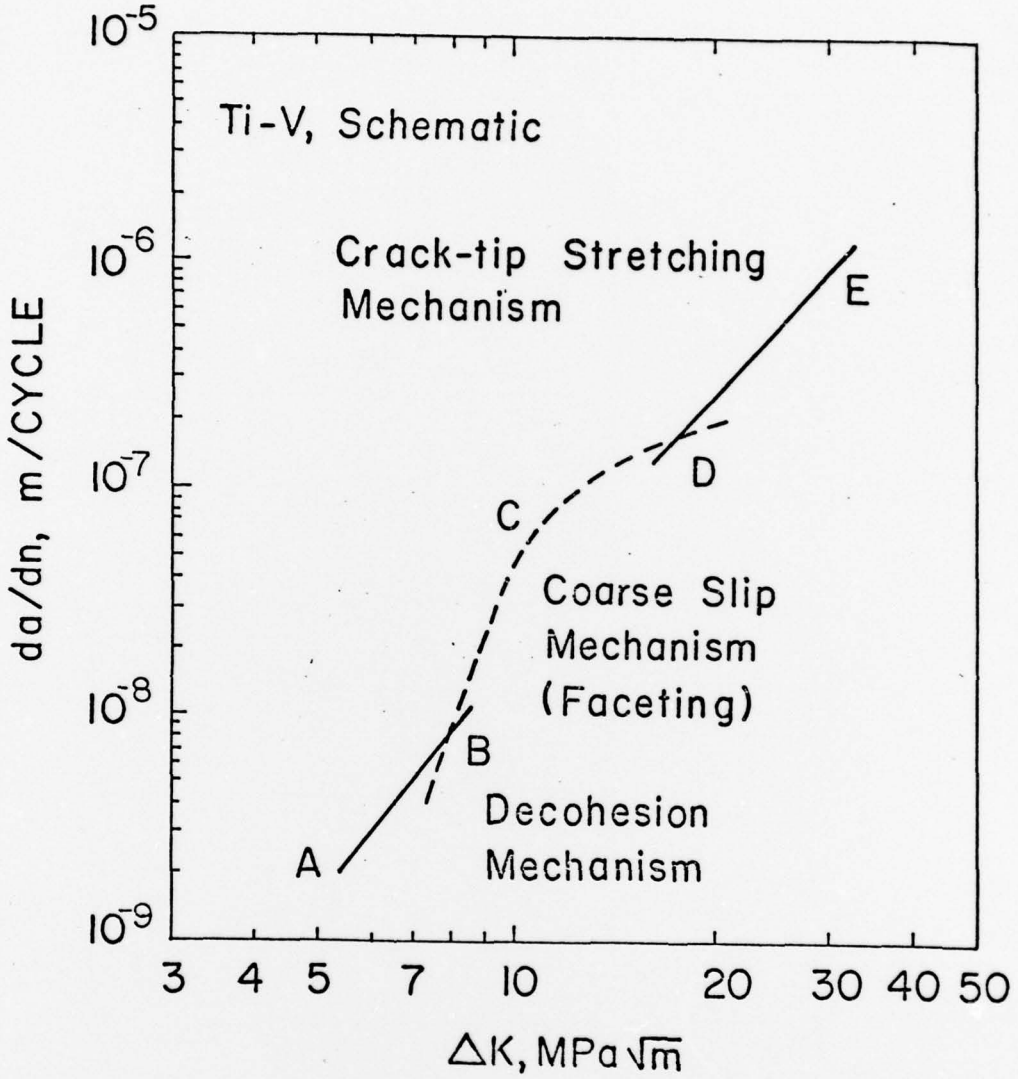

Figure 11: Schematic representation of the FCGR contributions from the three crack growth mechanisms for a typical beta Ti-V alloy.

SECURITY CLASSIFICATION OF THIS PAGE (When Data Entered)

REPORT DOCUMENTATION PAGE

READ INSTRUCTIONS BEFORE COMPLETING FORM

1. REPORT NUMBER: 78-3

2. GOVT ACCESSION NO.:

3. RECIPIENT'S CATALOG NUMBER:

4. TITLE (and Subtitle): Fatigue Crack Propagation of Metastable Beta Titanium-Vanadium Alloys.

5. TYPE OF REPORT & PERIOD COVERED: Technical Report

6. PERFORMING ORG. REPORT NUMBER:

7. AUTHOR(s): Saghana B. Chakraborty and Edgar A. Starke, Jr.

8. CONTRACT OR GRANT NUMBER(s): N00014-75-C-0349, NR 031-75

9. PERFORMING ORGANIZATION NAME AND ADDRESS:
Fracture and Fatigue Research Laboratory
Georgia Institute of Technology
Atlanta, GA 30332

10. PROGRAM ELEMENT, PROJECT, TASK AREA & WORK UNIT NUMBERS:

11. 7 Dec 76

11. CONTROLLING OFFICE NAME AND ADDRESS:
Metallurgy Program, Office of Naval Research
800 North Quincy Street
Arlington, Virginia 22217

12. REPORT DATE: December 7, 1978

13. NUMBER OF PAGES: 12 37p.

14. MONITORING AGENCY NAME & ADDRESS (if different from Controlling Office): 14 GIT-TR-78-3

15. SECURITY CLASS. (of this report): Unclassified

15a. DECLASSIFICATION/DOWNGRADING SCHEDULE:

16. DISTRIBUTION STATEMENT (of this Report):

unlimited

DISTRIBUTION STATEMENT A
Approved for public release;
Distribution Unlimited

17. DISTRIBUTION STATEMENT (of the abstract entered in Block 20, if different from Report)

18. SUPPLEMENTARY NOTES

19. KEY WORDS (Continue on reverse side if necessary and identify by block number)
titanium alloys
deformation
microstructure
fatigue

20. ABSTRACT (Continue on reverse side if necessary and identify by block number)

The fatigue crack propagation behavior of three titanium-vanadium alloys (24, 28 and 32 wt.% V) which have (tensile) deformation modes ranging from coarse twinning to wavy and planar slip has been measured in laboratory air and correlated with their low cycle fatigue properties and microstructure. The fatigue crack growth rate of alloys with similar microstructures but different deformation modes, and of alloys with similar deformation modes but different microstructures have been compared. Increasing the deformation barrier mean free path and improving low cycle fatigue properties has been observed to reduce the fatigue

DD FORM 1 JAN 73 1473 EDITION OF 1 NOV 65 IS OBSOLETE

411 058

JOB

SECURITY CLASSIFICATION OF THIS PAGE (When Data Entered)

crack growth rate at low and intermediate ΔK levels. The fatigue crack growth data have been compared with that calculated from equations which use microstructure and low cycle fatigue parameters. The predictive capability of these equations which contain only measurable parameters has been found to be quite adequate.